THE JOURNAL OF PHYSICAL CHEMISTRY LETTERS
A JOURNAL OF THE AMERICAN CHEMICAL SOCIETY

pubs.acs.org/JPCL
Letter

Direct, Indirect, and Self-Trapped Excitons in $Cs_2AgBiBr_6$

Mehmet Baskurt, Paul Erhart, and Julia Wiktor*

Cite This: J. Phys. Chem. Lett. 2024, 15, 8549−8554
Read Online

ABSTRACT: $Cs_2AgBiBr_6$ exhibits promising photovoltaic and light-emitting properties, making it a candidate for next-generation solar cells and LED technologies. Additionally, it serves as a model system within the family of halide double perovskites, offering insights into a broader class of materials. Here, we study various possible excited states of this material to understand its absorption and emission properties. We use time-dependent density functional theory (TD-DFT) coupled with nonempirical hybrid functionals, specifically PBE0(α) and dielectric-dependent hybrids (DDH) to explore direct, indirect, and self-trapped excitons in this material. Based on comparison with experiment, we show that these methods can give excellent predictions of the absorption spectrum and that the fundamental band gap has been underestimated in previous computational studies. We connect the experimental photoluminescence signals at 1.9−2.0 eV to the emission from self-trapped excitons and electron polarons. Finally, we reveal a complex landscape with energetically competing direct, indirect, and self-trapped excitons in the material.

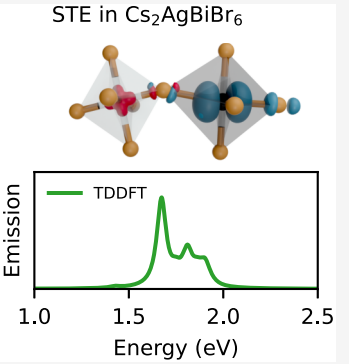

Halide perovskites (HPs), materials with the general ABX_3 formula, have attracted significant interest for their advanced optoelectronic applications, including solar panels and lighting. A subclass within the HP family, halide double perovskites, replaces the single B metal cation with a combination of two different elements, yielding the $A_2BB'X_6$ formula. Also known as elpasolites, these materials hold the potential for applications in photovoltaics, X-ray detection, and white light emission. Among halide double perovskites, $Cs_2AgBiBr_6$ stands out as one of the most studied. It has gained interest as a viable alternative to lead-based perovskites due to its high stability, nontoxicity, outstanding optoelectronic properties, and multifunctionality. Additionally, it has emerged as a benchmark case for both experimental and computational studies.

One of the interesting properties of halide double perovskites is that they often exhibit significant light emission. In $Cs_2AgBiBr_6$, a photoluminescence (PL) peak has been measured at 1.9−2.0 eV.[1−3] This emission has been assigned to the indirect band gap[2,4,5] or subgap states[6] such as color-centers.[1,3] It is therefore useful to computationally assess the likelihood of different sources of emission. Since the possible interpretations involve both free (in particular indirect) excitons and self-trapping, such a comparison requires a method that can model energetics of delocalized and localized excitations on the same footing.

The study of excited states requires methods extending beyond the density functional theory (DFT), such as the Bethe−Salpeter equation (BSE).[7−11] However, the high computational cost of BSE makes its use impractical in the case of self-trapped excitons (STEs), which in the most commonly used approach require the use of supercells. One notable exception is a study by Ismail-Beigi et al.[12] on the STE in SiO_2. We note that recent developments by Dai et al.[13,14] made it possible to model STEs in unit cells. However, this technique has not yet been widely applied and in the present study we want to focus on a cubic perovskite phase, which has been shown to be impossible to describe completely using a small symmetric structure.[15−17] Alternatively, recent advancements have allowed for more computationally efficient alternatives without compromising the accuracy inherent in BSE. Most notably, the combination of time-dependent density functional theory (TD-DFT) with nonempirical hybrid functionals has been shown to achieve the accuracy of BSE at a fraction of the cost.[18,19] While this method so far has been used for pristine materials and free excitons, its predictive power and relatively high computational efficiency make it a promising method for studying STEs as well. In a recent study by Jin et al.[20] it has been shown that STEs can be efficiently studied using the TD-DFT method. At the same time, they showed that the constrained-occupation DFT method, also called ΔSCF, leads to very similar geometries using TD-DFT forces to relax the structure of the STE.

In the present study, we combine TD-DFT with two types of nonempirical hybrid functionals. One is based on the PBE0(α) functional where the fraction of exact exchange α is set to a value which satisfies the generalized Koopmans'

Received: May 30, 2024
Revised: July 18, 2024
Accepted: August 5, 2024

https://doi.org/10.1021/acs.jpclett.4c01604
J. Phys. Chem. Lett. 2024, 15, 8549−8554

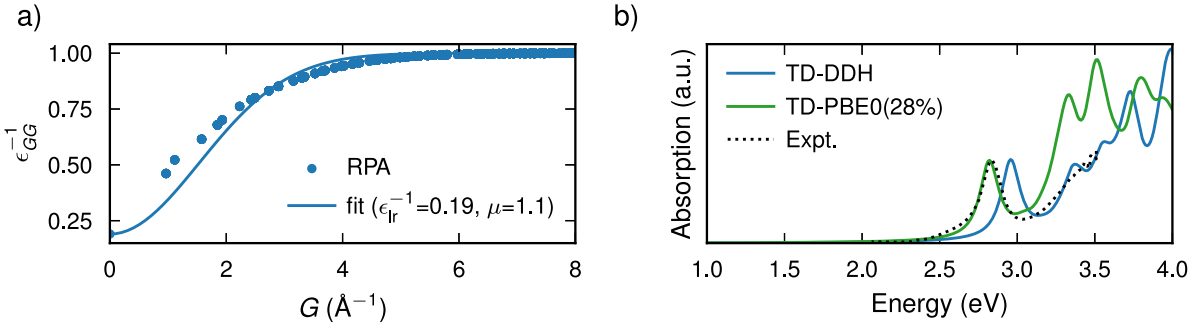

Figure 1. (a) Inverse dielectric function versus wave vector at the Γ point calculated within the RPA and fitted with eq 1. (b) Absorption spectra calculated using TD-DDH and TD-PBE0(28%) compared with the experimental results from ref 27. Computed absorption spectra include a convolution with Lorentzians with a width of 0.07 eV and were renormalized to match the intensity of the first experimental peak.

condition.[21−23] Another one belongs to the class of dielectric-dependent hybrid functionals (DDH),[24−26] in which the exchange potential follows the inverse of the dielectric function. From these methods, we extract the transitions of the direct and indirect free excitons as well as of the self-trapped exciton in the singlet and triplet state. We show that different excited states can be close in energy, and by performing careful convergence studies, we obtain the emission energy from the singlet state of the STE close to the experimental PL signal.

Calculations are performed using two simulation cells. Parametrization of the DDH functional, most convergence tests, and the comparison with the experimental absorption spectra are based on the unit cell of $Cs_2AgBiBr_6$ (space group $Fm\bar{3}m$) using the experimental lattice parameter of 11.27 Å.[28] Calculations for the free excitons and the STE are done in a supercell containing 320 atoms, based on the polymorphous cubic structure[16] from ref 23, where we used the ΔSCF method for the excited state. In that work, we studied charge localization in $Cs_2AgBiBr_6$ and showed that small electron polarons and STEs are stable in the material, while the localization of small hole polarons is less favorable. We note that these results align well with the later findings by Lafuente-Bartolome et al.[29] From ref 23, we adopt the α parameter in PBE0(α) of 0.28, which has been shown to satisfy the Koopmans' condition for the Br vacancy. All simulations presented in the main text include spin−orbit coupling (SOC), while some of the convergence tests shown in the Supporting Information are done without this contribution. Additional computational details and convergence tests can be found in the Supporting Information.

We first calculate the dielectric function ϵ of $Cs_2AgBiBr_6$ within the random-phase approximation (RPA). The calculation is carried out using an energy cutoff of 400 eV and a k-point mesh of 6 × 6 × 6. As shown in the Supporting Information, these parameters lead to a very well converged dielectric function. The result is given in Figure 1a in which we also include the fit following

$$\epsilon^{-1}(G) = 1 - (1 - \epsilon_{lr}^{-1})e^{-G^2/(4\mu^2)} \quad (1)$$

where ϵ_{lr}^{-1} corresponds to the long-range exchange fraction at $G = 0$, G is the wave vector, and μ is the range-separation parameter. We obtain $\epsilon_{lr}^{-1} = 0.19$ and $\mu = 1.1$.

To verify the validity of our hybrid functionals, we compare the absorption spectra calculated via TD-DFT with experimental results from ref 3 (see Figure 1b). The absorption α_{abs} is calculated based on the real and imaginary parts of the dielectric function ϵ as

$$\alpha_{abs}(\omega) = \sqrt{2}\frac{\omega}{c}\sqrt{|\epsilon(\omega)| - \epsilon_R(\omega)} \quad (2)$$

where c is the speed of light and ω is the angular frequency.[30] Convergence tests corresponding to the TD-DFT calculations are given in the Supporting Information. We observe a good agreement with the experimental results using both hybrid functionals, with TD-PBE0(28%) reproducing the position of the first absorption peak almost exactly and TD-DDH slightly overestimating it, while giving a better agreement for the valley and the second peak. We attribute the overestimation of the second peak within TD-PBE0(28%) to its incorrect asymptotic behavior. Using the nonempirical hybrid functionals, we obtain a much better agreement with experimental data than previous G_0W_0 calculations,[31] where the position of the first peak was underestimated by about 0.6 eV. This is due to the fact that while nonempirical hybrid functionals have been shown to give high accuracy in describing band gaps of halide perovskites,[22,32] the one-shot G_0W_0 used in ref 31 can significantly underestimate that property.[15,33,34] The authors of ref 31 noted that this underestimation is primarily due to the lack of self-consistency and the starting point dependence of G_0W_0 calculations, which is a well-known issue. Although other calculations in ref 5 considered partial self-consistency by updating energies in G and W (the *evGW* scheme), this approach still did not lead to the full increase of the band gap that would reproduce experimental results. In Table 1 we include the fundamental direct and indirect gaps calculated with the DDH and PBE0(α) methods and compare them with previous computationally reported values (the band structure

Table 1. Fundamental Indirect and Direct Band Gaps from the PBE0(α) and DDH Functionals Compared with Previously Reported Values

	indirect gap (eV)	direct gap (eV)
PBE0(28%)	2.66	3.52
DDH	2.66	3.50
DSH ref 35	2.50	
G_0W_0@LDA ref 36	1.83	2.51
G_0W_0@PBE ref 34	2.01	
G_0W_0@LDA ref 31	1.66	2.41
G_0W_0@HSE ref 34	2.59	
GW_0@HSE ref 34	2.82	
evGW ref 5	2.1	2.7

https://doi.org/10.1021/acs.jpclett.4c01604
J. Phys. Chem. Lett. 2024, 15, 8549−8554

is given in the Supporting Information). First, we note that the two hybrid functionals constructed by using different physical considerations lead to almost the same indirect and direct band gaps. Our indirect band gap is also close to the value recently calculated by Wang et al. using the double screened hybrid (DSH) functional.[35] Second, even when similar methods are employed, such as G_0W_0 on top of LDA or PBE, band gaps can differ by as much as 0.35 eV. This discrepancy can be attributed to differences in the underlying functional, codes used, the choice between PAW and norm-conserving pseudopotentials, and the selection of valence states. Third, we observe that the values present here, about 2.7 and 3.5 eV for the indirect and direct transitions, respectively, are higher than most previous estimates. However, considering the excellent agreement between absorption spectra calculated here and the experiment, we argue that the presented fundamental gaps are more reliable predictions than the previously reported values.

The previous calculations were performed for the perfect cubic structure of $Cs_2AgBiBr_6$. It has been shown that such a symmetric model is not a good representation of the locally and dynamically disordered halide perovskites.[15−17] We note that ref 37 has shown that unlike lead-based perovskites, $Cs_2AgBiBr_6$ has well-defined normal modes up to room temperature, which means that the symmetric average cubic structure is enough to describe the electronic structure of the material even at finite temperatures. We demonstrate this by comparing the imaginary part of the dielectric function calculated within the pristine $Fm\bar{3}m$ unit cell and the polymorphous supercell in the Supporting Information. However, introducing local distortions within the perfect cubic supercell would lead to its relaxation to a form of a polymorphous cell or to finding a local minimum where the optimal charge localization is not possible.[23] Therefore, we now turn to the study of the excited states of $Cs_2AgBiBr_6$ based on a more realistic polymorphous model. We adopt one polymorphous structure for the pristine $Cs_2AgBiBr_6$ and one for the STE from ref 23. We note that we have also tested how the properties of the STE change when the low-temparature tetragonal structure ($I4/m$) is considered and found that similar transitions can be found in that model (see Supporting Information for the test). These structures were generated using the CP2K code,[38,39] and here, for consistency, we further relax the atomic position within VASP. In the following, we focus on the PBE0(28%) functional, as it gives a slightly better agreement with experiment for the lower part of the absorption spectrum. The STE is relaxed within its lowest triplet state, and we assume that the atomic positions do not change significantly for the singlet state. We show the isodensities of the localized hole and electron in Figure 2a). We then perform TD-DFT calculations using the two hybrid functionals on top of these geometries. While the relaxation is performed using the Γ point only, for the TD-DFT calculations we use a special grid with four k-points. As shown in the Supporting Information, this grid yields lower parts of the absorption spectra that agree well with those from the $2 \times 2 \times 2$ grid. The differences in the positions of the two lowest peaks between the two grids are below 0.03 eV. In the pristine material, we observe the lowest transition at 2.45 eV. This transition is dark and corresponds to the lowest indirect exciton. It would not be captured in the unit cell, unless momentum transfers are considered as in ref 5. However, in the supercell used in this study, the X and L points are folded onto the Γ point and are

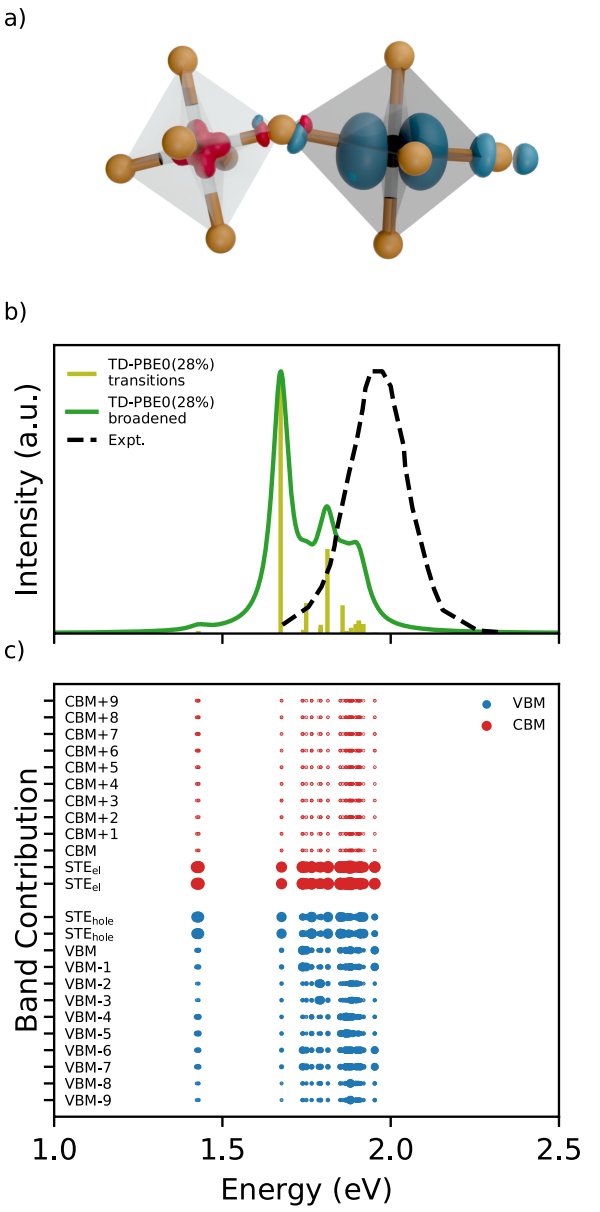

Figure 2. (a) Isodensities of the hole (in red) and electron (in blue), localized within the $AgBr_6$ and $BiBr_6$ octahedron, respectively. The rest of the structure was removed for clarity. (b) Emission from the STE compared with the experimental PL spectrum from ref 3. The broadened spectrum was generated by convolution with Lorentzians with a width of 0.03 eV. All spectra were rescaled to have the same maximum. (c) Band contributions to each of the transitions marked in the upper panel. For each initial (final) state, the contributions of different final (initial) states, as well as all k-points, are added up.

directly accessible by TD-DFT. From the difference between this dark transition and the fundamental band gap in the polymorphous supercell of 2.83 eV we estimate the binding energy of the lowest indirect free exciton to be 0.39 eV. This is slightly lower than the value of 0.48 eV, reported by Palummo et al.[5] The first bright transition, corresponding to the lowest direct free exciton is found at 2.96 eV, while the lowest direct independent-particle transition equals 3.57 eV in the same setup. This implies the binding energy of the direct exciton of 0.61 eV. Within the unit cell, we find the binding energy to amount to 0.55 eV (see the related discussion in Supporting Information). We note that this value is significantly higher

https://doi.org/10.1021/acs.jpclett.4c01604
J. Phys. Chem. Lett. 2024, 15, 8549−8554

than previously reported ones (0.34 eV in ref 5 and 0.17 eV in ref 31), which can be assigned to the higher fundamental band gap of $Cs_2AgBiBr_6$ in the present setup. In their study, Biega et al.[31] demonstrated a linear relationship between the exciton binding energy and the size of the direct band gap, which would explain the higher value found here. In the Supporting Information we also demonstrate that by reducing the amount of exact exchange in the PBE0 functional, the exciton binding energy is reduced and in good agreement with previous studies in which the band gaps were also found to be smaller.

We now analyze the transitions in the TD-DFT calculations for the STE geometry. We note that the calculation corresponds to the excitation from the singlet ground state. However, since absorption and emission are inverse processes, the calculated energy transitions can be expected to be directly comparable to measured photoluminescence spectra. The calculated transitions of the STE are given in Figure 2b. While TD-DFT gives all transitions, we only plot those below 2 eV, as they correspond to the energy range in which photoluminescence is measured. We compare the results with the experimental PL spectrum from ref 3. The measurement was done at 4 K; hence, the phonon broadening can be neglected in the comparison. While the simulated spectrum is at lower energies than the experimental one, the difference between the midpoints of the spectra is only about 0.2 eV, representing fairly good agreement. We also note that the broadness of the experimental peak at low temperatures can be explained by the distribution of transitions that contribute to it. Previous works also suggested the possibility that the experimental emission is due to the indirect band gap[2,4,5] or subgap states[6] such as color-centers.[1,3] We rule out emission from the indirect band gap based on two arguments. First, we find this transition at a significantly higher energy, 2.49 eV. Second, this type of recombination requires an additional momentum change to occur. As for defects, to contribute to the emission, they would need to be deep and trap charges more strongly than STE or small polarons. In that case, they would also lead to transitions at even lower energies than what we report here. In Figure 2c we show the band composition of the calculated transitions. The lowest transition at 1.42 eV has a very low intensity and corresponds to a spin-forbidden triplet-singlet transition between the localized electron and hole states from within the STE. Then, at 1.68 eV there is a bright transition from the singlet state of the STE. This implies a separation of 0.26 eV between the lowest triplet and higher singlet states of the STE in $Cs_2AgBiBr_6$. At higher energies, between 1.74 and 1.95 eV, there is a distribution of transitions which all involve the localized electron state and both localized and delocalized hole states. This range of energies can be used as an estimate of PL stemming from the electron polaron if the STE dissociates. In this energy range, we do not observe any transitions between the localized hole and delocalized electrons because the hole in the STE has a more shallow level than the electron, and this type of emission would mostly overlap with the absorption onset close to 3 eV.

Using the energy transitions from the TD-DFT calculations, we finally construct the configuration coordinate diagram. It allows us to compare the energies of direct, indirect, and self-trapped excitons. The diagram, given in Figure 3, is based on TD-PBE0(28%) calculations in the polymorphous cubic supercell. The energies at the ground-state and STE geometries are explicitly calculated and connected by parabolic curves to schematically represent the energy dependence on displacement. The diagram reveals a complex landscape of electron−hole excitations in the material and can be used to analyze the dynamics of the excited charges. First, direct free excitons are created. These free excitons can then be trapped in the form of the singlet STE. This STE can then undergo four processes. One, it can recombine, leading to a bright emission that can be measured in photoluminescence. Two, it can lower its energy and turn into a triplet form of STE. Three, it can detrap and become an indirect free exciton, which has an energy very close to that of the triplet STE (within 0.1 eV in the current computational setup). Finally, it could also dissociate leaving behind a localized electron and possibly a delocalized hole.[23] We note that this diagram provides a more comprehensive picture of the energetics involved compared to ref 23, which only compared the energy of the triplet STE with the lowest indirect free-carrier transition.

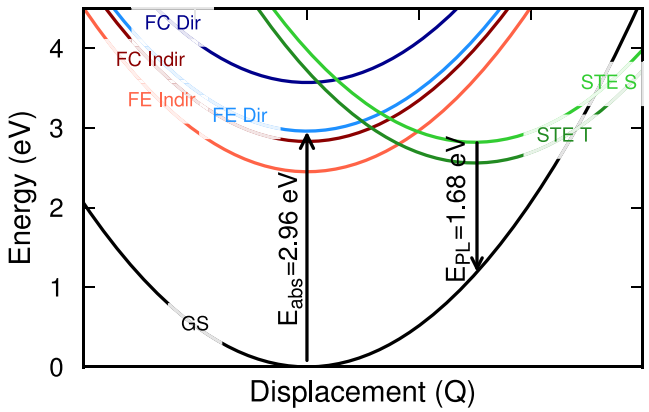

Figure 3. Configuration coordinate diagram of different electron−hole pairs in $Cs_2AgBiBr_6$, including free carriers (FC), free excitons (FE), and self-trapped excitons (STE). "Indir" and "Dir" refer to indirect and direct transitions, and "S" and "T" refer to singlet and triplet states.

In conclusion, we have studied different types of excitons in $Cs_2AgBiBr_6$ halide double perovskites. We first assessed the performance of two nonempirical hybrid functionals, PBE0(28%) and DDH in the description of the optical properties of the pristine material. We have shown that both of them predict band gaps higher than what was previously reported in the literature and give absorption spectra in very good agreement with experiment. We then used the TD-PBE0(28%) technique to study excitations in the polymorphous cubic supercells corresponding to the ground-state structure and the self-trapped exciton. This allowed us to show that the emission from the STE is in good agreement with experimental PL spectra. Based on a configuration coordinate diagram, we finally revealed a complex landscape of electron−hole pairs in the materials with direct, indirect, and self-trapped excitons having comparable energies.

■ ASSOCIATED CONTENT

Data Availability Statement

Structures of the pristine material and of the self-trapped exciton are publicly available via Zenodo at https://doi.org/10.5281/zenodo.13258153.

Supporting Information

The Supporting Information is available free of charge at https://pubs.acs.org/doi/10.1021/acs.jpclett.4c01604.

https://doi.org/10.1021/acs.jpclett.4c01604
J. Phys. Chem. Lett. 2024, 15, 8549−8554

Computational details, band structure of $Cs_2AgBiBr_6$, and convergence tests (PDF)

AUTHOR INFORMATION

Corresponding Author

Julia Wiktor − *Department of Physics, Chalmers University of Technology, 41296 Gothenburg, Sweden;* orcid.org/0000-0003-3395-1104; Email: julia.wiktor@chalmers.se

Authors

Mehmet Baskurt − *Department of Physics, Chalmers University of Technology, 41296 Gothenburg, Sweden;* orcid.org/0000-0001-7181-6814

Paul Erhart − *Department of Physics, Chalmers University of Technology, 41296 Gothenburg, Sweden;* orcid.org/0000-0002-2516-6061

Complete contact information is available at: https://pubs.acs.org/10.1021/acs.jpclett.4c01604

Notes

The authors declare no competing financial interest.

ACKNOWLEDGMENTS

This work was supported by the Swedish Research Council (Grants 2019-03993 and 2020-04935), the Swedish Strategic Research Foundation through a Future Research Leader program (Grant FFL21-0129), and the Wallenberg Academy Fellow program. The computations were enabled by resources provided by the National Academic Infrastructure for Supercomputing in Sweden (NAISS) at C3SE, NSC, and PDC partially funded by the Swedish Research Council through Grant Agreements 2022-06725 and 2018-05973.

REFERENCES

(1) Zelewski, S.; Urban, J.; Surrente, A.; Maude, D. K.; Kuc, A.; Schade, L.; Johnson, R.; Dollmann, M.; Nayak, P.; Snaith, H.; et al. Revealing the Nature of Photoluminescence Emission in the Metal-Halide Double Perovskite $Cs_2AgBiBr_6$. *J. Mater. Chem. C* **2019**, *7*, 8350−8356.

(2) Schade, L.; Wright, A. D.; Johnson, R. D.; Dollmann, M.; Wenger, B.; Nayak, P. K.; Prabhakaran, D.; Herz, L. M.; Nicholas, R.; Snaith, H. J.; et al. Structural and Optical Properties of $Cs_2AgBiBr_6$ Double Perovskite. *ACS Energy Lett.* **2019**, *4*, 299−305.

(3) Wright, A. D.; Buizza, L. R.; Savill, K. J.; Longo, G.; Snaith, H. J.; Johnston, M. B.; Herz, L. M. Ultrafast Excited-State Localization in $Cs_2AgBiBr_6$ Double Perovskite. *J. Phys. Chem. Lett.* **2021**, *12*, 3352−3360.

(4) Slavney, A. H.; Hu, T.; Lindenberg, A. M.; Karunadasa, H. I. A Bismuth-Halide Double Perovskite with Long Carrier Recombination Lifetime for Photovoltaic Applications. *J. Am. Chem. Soc.* **2016**, *138*, 2138−2141.

(5) Palummo, M.; Berrios, E.; Varsano, D.; Giorgi, G. Optical Properties of Lead-Free Double Perovskites by Ab Initio Excited-State Methods. *ACS Energy Lett.* **2020**, *5*, 457−463.

(6) Hoye, R. L.; Eyre, L.; Wei, F.; Brivio, F.; Sadhanala, A.; Sun, S.; Li, W.; Zhang, K. H.; MacManus-Driscoll, J. L.; Bristowe, P. D.; et al. Fundamental Carrier Lifetime Exceeding 1 μs in $Cs_2AgBiBr_6$ Double Perovskite. *Adv. Mater. Interfaces* **2018**, *5*, 1800464.

(7) Albrecht, S.; Reining, L.; Del Sole, R.; Onida, G. Ab Initio Calculation of Excitonic Effects in the Optical Spectra of Semiconductors. *Phys. Rev. Lett.* **1998**, *80*, 4510.

(8) Rohlfing, M.; Louie, S. G. Excitonic Effects and the Optical Absorption Spectrum of Hydrogenated Si Clusters. *Phys. Rev. Lett.* **1998**, *80*, 3320.

(9) Benedict, L. X.; Shirley, E. L.; Bohn, R. B. Optical Absorption of Insulators and the Electron-Hole Interaction: An Ab Initio Calculation. *Phys. Rev. Lett.* **1998**, *80*, 4514.

(10) Onida, G.; Reining, L.; Rubio, A. Electronic Excitations: Density-Functional Versus Many-Body Green's-Function Approaches. *Rev. Mod. Phys.* **2002**, *74*, 601.

(11) Sun, H.-Y.; Xiong, L.; Jiang, H. Toward First-Principles Approaches for Mechanistic Study of Self-Trapped Exciton Luminescence. *Chem. Phys. Rev.* **2023**, *4*, 031302.

(12) Ismail-Beigi, S.; Louie, S. G. Self-Trapped Excitons in Silicon Dioxide: Mechanism and Properties. *Phys. Rev. Lett.* **2005**, *95*, 156401.

(13) Dai, Z.; Lian, C.; Lafuente-Bartolome, J.; Giustino, F. Excitonic Polarons and Self-Trapped Excitons from First-Principles Exciton-Phonon Couplings. *Phys. Rev. Lett.* **2024**, *132*, 036902.

(14) Dai, Z.; Lian, C.; Lafuente-Bartolome, J.; Giustino, F. Theory of Excitonic Polarons: From Models to First-Principles Calculations. *Phys. Rev. B* **2024**, *109*, 045202.

(15) Wiktor, J.; Rothlisberger, U.; Pasquarello, A. Predictive Determination of Band Gaps of Inorganic Halide Perovskites. *J. Phys. Chem. Lett.* **2017**, *8*, 5507−5512.

(16) Zhao, X.-G.; Dalpian, G. M.; Wang, Z.; Zunger, A. Polymorphous Nature of Cubic Halide Perovskites. *Phys. Rev. B* **2020**, *101*, 155137.

(17) Wiktor, J.; Fransson, E.; Kubicki, D.; Erhart, P. Quantifying Dynamic Tilting in Halide Perovskites: Chemical Trends and Local Correlations. *Chem. Mater.* **2023**, *35*, 6737−6744.

(18) Sun, J.; Yang, J.; Ullrich, C. A. Low-Cost Alternatives to the Bethe-Salpeter Equation: Towards Simple Hybrid Functionals for Excitonic Effects in Solids. *Phys. Rev. Res.* **2020**, *2*, 013091.

(19) Tal, A.; Liu, P.; Kresse, G.; Pasquarello, A. Accurate Optical Spectra Through Time-Dependent Density Functional Theory Based on Screening-Dependent Hybrid Functionals. *Phys. Rev. Res.* **2020**, *2*, 032019.

(20) Jin, Y.; Rusishvili, M.; Govoni, M.; Galli, G. Self-Trapped Excitons in Metal-Halide Perovskites Investigated by Time-Dependent Density Functional Theory. *J. Phys. Chem. Lett.* **2024**, *15*, 3229−3237.

(21) Dabo, I.; Ferretti, A.; Poilvert, N.; Li, Y.; Marzari, N.; Cococcioni, M. Koopmans' Condition for Density-Functional Theory. *Phys. Rev. B* **2010**, *82*, 115121.

(22) Bischoff, T.; Wiktor, J.; Chen, W.; Pasquarello, A. Nonempirical Hybrid Functionals for Band Gaps of Inorganic Metal-Halide Perovskites. *Phys. Rev. Mater.* **2019**, *3*, 123802.

(23) Baskurt, M.; Wiktor, J. Charge Localization in $Cs_2AgBiBr_6$ Double Perovskite: Small Polarons and Self-Trapped Excitons. *J. Phys. Chem. C* **2023**, *127*, 23966−23972.

(24) Chen, W.; Miceli, G.; Rignanese, G.-M.; Pasquarello, A. Nonempirical Dielectric-Dependent Hybrid Functional with Range Separation for Semiconductors and Insulators. *Phys. Rev. Mater.* **2018**, *2*, 073803.

(25) Cui, Z.-H.; Wang, Y.-C.; Zhang, M.-Y.; Xu, X.; Jiang, H. Doubly Screened Hybrid Functional: An Accurate First-Principles Approach for Both Narrow-and Wide-Gap Semiconductors. *J. Phys. Chem. Lett.* **2018**, *9*, 2338−2345.

(26) Liu, P.; Franchini, C.; Marsman, M.; Kresse, G. Assessing Model-Dielectric-Dependent Hybrid Functionals on the Antiferromagnetic Transition-Metal Monoxides MnO, FeO, CoO, and NiO. *J. Phys.: Condens. Matter* **2020**, *32*, 015502.

(27) Longo, G.; Mahesh, S.; Buizza, L. R.; Wright, A. D.; Ramadan, A. J.; Abdi-Jalebi, M.; Nayak, P. K.; Herz, L. M.; Snaith, H. J. Understanding the Performance-Limiting Factors of $Cs_2AgBiBr_6$ Double-Perovskite Solar Cells. *ACS Energy Lett.* **2020**, *5*, 2200−2207.

(28) Ning, W.; Bao, J.; Puttisong, Y.; Moro, F.; Kobera, L.; Shimono, S.; Wang, L.; Ji, F.; Cuartero, M.; Kawaguchi, S.; et al. Magnetizing Lead-Free Halide Double Perovskites. *Sci. Adv.* **2020**, *6*, No. eabb5381.

(29) Lafuente-Bartolome, J.; Lian, C.; Giustino, F. Topological Polarons in Halide Perovskites. *Proc. Natl. Acad. Sci. U.S.A.* **2024**, *121*, No. e2318151121.
(30) Sadigh, B.; Erhart, P.; Åberg, D.; Trave, A.; Schwegler, E.; Bude, J. First-Principles Calculations of the Urbach Tail in the Optical Absorption Spectra of Silica Glass. *Phys. Rev. Lett.* **2011**, *106*, 027401.
(31) Biega, R.-I.; Filip, M. R.; Leppert, L.; Neaton, J. B. Chemically Localized Resonant Excitons in Silver−Pnictogen Halide Double Perovskites. *J. Phys. Chem. Lett.* **2021**, *12*, 2057−2063.
(32) Wang, H.; Tal, A.; Bischoff, T.; Gono, P.; Pasquarello, A. Accurate and Efficient Band-Gap Predictions for Metal Halide Perovskites at Finite Temperature. *npj Comput. Mater.* **2022**, *8*, 237.
(33) Filip, M. R.; Giustino, F. G W. Quasiparticle Band Gap of the Hybrid Organic-Inorganic Perovskite $CH_3NH_3PbI_3$: Effect of Spin-Orbit Interaction, Semicore Electrons, and Self-Consistency. *Phys. Rev. B* **2014**, *90*, 245145.
(34) Leppert, L.; Rangel, T.; Neaton, J. B. Towards Predictive Band Gaps for Halide Perovskites: Lessons from One-Shot and Eigenvalue Self-Consistent G W. *Phys. Rev. Mater.* **2019**, *3*, 103803.
(35) Wang, H.; Ouyang, R.; Chen, W.; Pasquarello, A. High-Quality Data Enabling Universality of Band Gap Descriptor and Discovery of Photovoltaic Perovskites. *J. Am. Chem. Soc.* **2024**, *146*, 17636.
(36) Filip, M. R.; Hillman, S.; Haghighirad, A. A.; Snaith, H. J.; Giustino, F. Band Gaps of the Lead-Free Halide Double Perovskites $Cs_2BiAgCl_6$ and $Cs_2BiAgBr_6$ from Theory and Experiment. *J. Phys. Chem. Lett.* **2016**, *7*, 2579−2585.
(37) Cohen, A.; Brenner, T. M.; Klarbring, J.; Sharma, R.; Fabini, D. H.; Korobko, R.; Nayak, P. K.; Hellman, O.; Yaffe, O. Diverging Expressions of Anharmonicity in Halide Perovskites. *Adv. Mater.* **2022**, *34*, 2107932.
(38) VandeVondele, J.; Krack, M.; Mohamed, F.; Parrinello, M.; Chassaing, T.; Hutter, J. Quickstep: Fast and Accurate Density Functional Calculations Using a Mixed Gaussian and Plane Waves Approach. *Comput. Phys. Commun.* **2005**, *167*, 103−128.
(39) Kühne, T. D.; Iannuzzi, M.; Del Ben, M.; Rybkin, V. V.; Seewald, P.; Stein, F.; Laino, T.; Khaliullin, R. Z.; Schütt, O.; Schiffmann, F.; et al. CP2K: An Electronic Structure and Molecular Dynamics Software Package-Quickstep: Efficient and Accurate Electronic Structure Calculations. *J. Chem. Phys.* **2020**, *152*, 194103.

https://doi.org/10.1021/acs.jpclett.4c01604
J. Phys. Chem. Lett. 2024, 15, 8549−8554

Supporting Information:

Direct, Indirect, and Self-Trapped Excitons in $Cs_2AgBiBr_6$

Mehmet Baskurt[1], Paul Erhart[1], and Julia Wiktor[1,*]

[1] *Department of Physics, Chalmers University of Technology, SE-41296, Gothenburg, Sweden*
[*] *julia.wiktor@chalmers.se*

1 Computational details

All calculations in the main text are performed using the Projector Augmented-Wave (PAW) method, as implemented in the VASP software package [1, 2]. The atomic positions in the unit cell were relaxed using the SCAN+rVV10 functional [3], which has been shown to provide very good predictions of the structural properties of halide perovskites [4]. The valence states considered are $5s^2 5p^6 6s^1$ for Cs, $4d^{10} 5s^1$ for Ag, $6s^2 6p^3$ for Bi, and $4s^2 4p^5$ for Br. In a recent study Wang *et al.* [5] showed that including semicore states has a significant effect on the band gap of $Cs_2AgBiBr_6$ when combining norm-conserving pseudopotentials and hybrid functionals. We verified that, when using the PAW method, including one additional shell among the valence states of Ag, Bi, and Br increases the band gap by only 0.08 eV and 0.05 eV with the DDH and PBE0(28%) functionals, respectively. Therefore, we conclude that the issue observed by Wang *et al.* is specific to norm-conserving pseudopotentials.

2 Band structure of $Cs_2AgBiBr_6$

$Cs_2AgBiBr_6$ is an indirect band gap semiconductor with the valence band maximum at the X point and the conduction band minimum at the L point. We plot the band structure of the material in Figure 1.

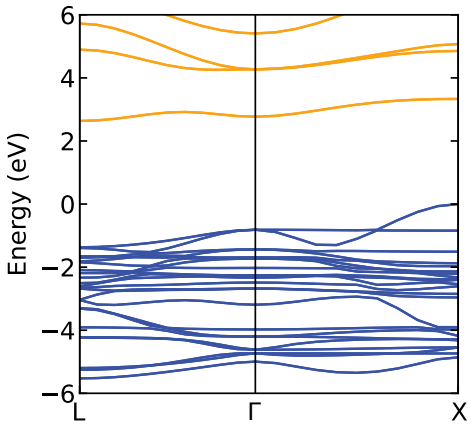

Figure 1: Band structure of $Cs_2AgBiBr_6$ calculated within the PBE0(28%) functional.

3 Convergence tests

We calculate the frequency-dependent dielectric function of $Cs_2AgBiBr_6$ in the unit cell within the Random Phase Approximation (RPA). We verify the convergence with the cutoff energy and the k-

point grid and find that the dielectric function is well converged with the grid of 4×4×4 and cutoff of 400 eV.

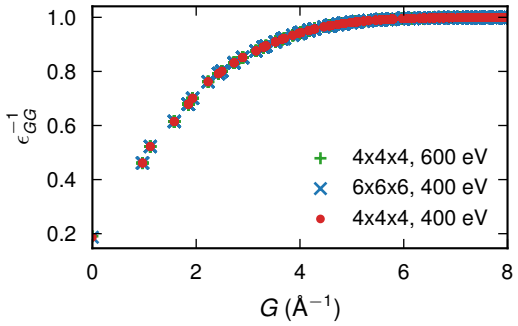

Figure 2: Convergence of the dielectric function with respect to the k-point grid and cutoff energy.

We evaluate the convergence of the absorption spectrum by calculating the imaginary part of the dielectric function within the TD-PBE0(28%) method in the unit cell with varying parameters. We find that the lower part of the spectrum is well converged using the cutoff of 200 eV, the k-point grid of 6×6×6 and considering 10 occupied and 10 unoccupied bands in the Casida equation. We note that all calculation include the Tamm-Dancoff approximation.

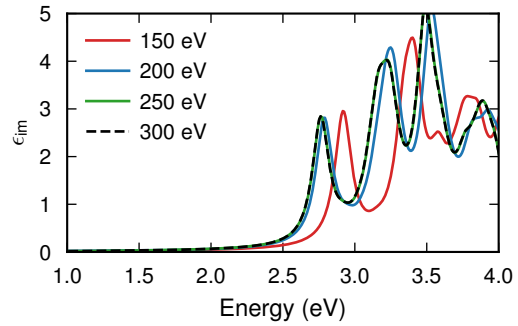

Figure 3: Convergence of the imaginary part of the dielectric function with respect to the cutoff energy.

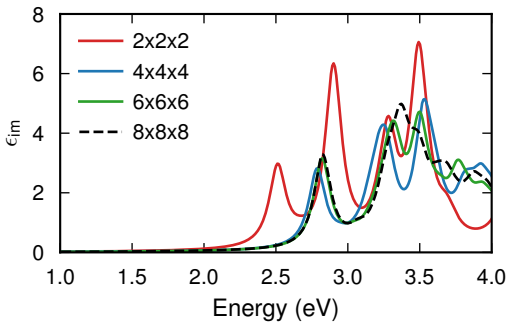

Figure 4: Convergence of the imaginary part of the dielectric function with respect to the k-point grid.

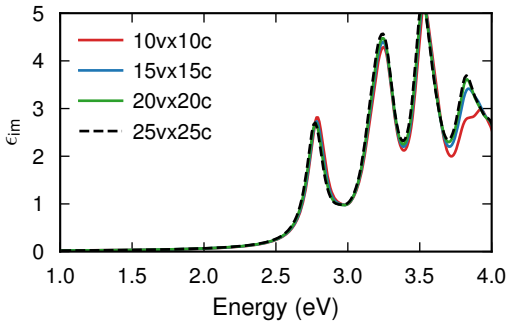

Figure 5: Convergence of the imaginary part of the dielectric function with respect to numbers of occupied and unoccupied bands included in the Casida equation.

We perform separate convergence tests for the supercell. While the cutoff energy is not affected by the cell size, we verify the convergence of the imaginary part of the dielectric function with respect to the k-point mesh and the number of occupied and unoccupied states in the Casida equation. To speed up the convergence with the number of k-points, we consider a special grid with 4 points at (0,0,0), (0,0.5,0.5), (0.5,0,0.5), and (0.5,0.5,0). This grid gives a dielectric function in good agreement with the $2\times2\times2$ grid and is used in the main text. We observe that increasing the density of k-points shifts the peaks in the imaginary part of the dielectric function to slightly higher energies. Conversely, increasing the number of states considered in the Casida equation shifts the peaks to lower energies. Therefore, we anticipate a significant cancellation of errors between these two convergence parameters. In the main text, we present the values calculated with the 4-point k-point grid and with 175 valence and conduction states.

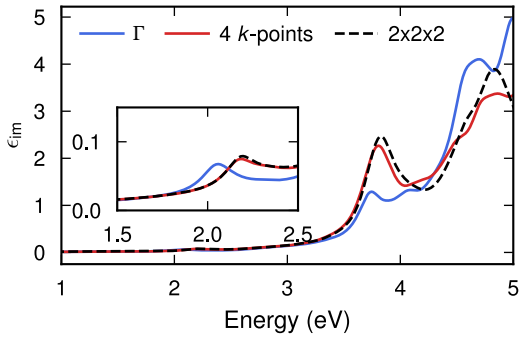

Figure 6: Convergence of the imaginary part of the dielectric function calculated in the geometry of the STE (on the ground state) with respect to the number of k-points. SOC effects have been excluded in this test.

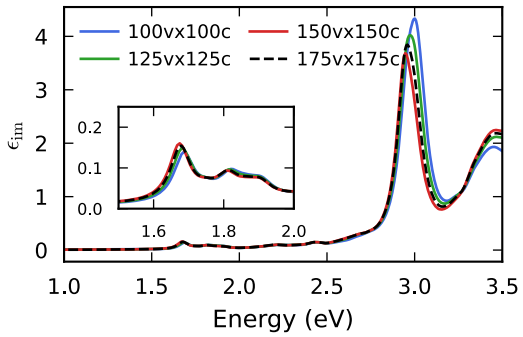

Figure 7: Convergence of the imaginary part of the dielectric function calculated in the geometry of the STE (on the ground state) with respect to the number of occupied and unoccupied bands included in the Casida equation. SOC effects are included in this test.

4 Effect of the fraction of exact exchange on the exciton binding energy

We find the exciton binding energy (E_b) of the first bright exciton (calculated with respect to the fundamental direct band gap) to amount to 550 and 420 meV in in TD-PBE0(28%) and TD-DDH, respectively, as calculated within the unit cell. These values are higher than the previous computational estimates of for example 170 meV in Ref. [6] and 340 meV in Ref. [7]. At the same time, it has been shown that the exciton binding energy is correlated with the band gap [6] and we here calculate larger band gap than in most previous studies. To demonstrate this relationship within our computational setup, we recalculate the exciton binding energies with the TD-PBE0(α) method, where we vary the amount of exact exchange α. Table S1 shows the dependence of E_b on α and the fundamental direct band gap $E_\mathrm{gap}^\mathrm{dir}$. We observe that with the smaller values of α the band gap is closer to what was calculated in Refs. [6] and [7], and so is the exciton binding energy.

Table S1: Exciton binding energy as a function of α and the band gap ($E_\mathrm{gap}^\mathrm{dir}$) in the TD-PBE0($\alpha$) calculations.

α	$E_\mathrm{gap}^\mathrm{dir}$ (eV)	E_b (meV)
10%	2.34	90
20%	2.90	290
28%	3.36	550

5 Absorption properties in the polymorphous supercell vs. unit cell

In the main text, we benchmark the computational setups by comparing the calculated absorption spectrum with the experimental data. These calculations are performed in the F$m\bar{3}m$ unit cell. The properties of the STE are then studied in a polymorphous supercell. We here test how the absorption of the pristine material compares within the polymorphous supercell and the unit cell. The comparison is given in Figure 8. We observe that when the atomic positions are relaxed with the same method (here SCAN+rVV10), the lower-energy parts of the dielectric function match well between the unit cell and the polymorphus cubic cell. When atomic positions in the polymorphous supercell are relaxed within PBE0(28%), the first peak is shifted by about 0.14 eV to higher energies. In the analysis of the energetics of the excited states in $Cs_2AgBiBr_6$ we consider calculations in which atomic position are relaxed with the PBE0(28%) method, as this is required to obtain the correct charge localization within the STE.

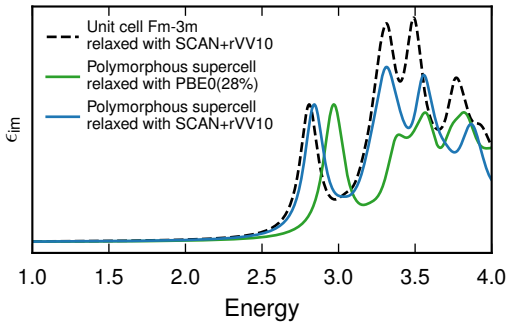

Figure 8: Comparison between the imaginary part of the dielectric function calculated within the F$m\bar{3}m$ unit cell (atomic positions relaxed with SCAN+rVV10) and the cubic supercell (atomic positions relaxed with PBE0(28%) and SCAN+rVV10, respectively). The dielectric functions include a convolution with Lorentzians with a width of 0.07 eV and were normalized to have the same intensity at the first peak.

6 STE in polymorphous vs. tetragonal cell

$Cs_2AgBiBr_6$ has, on average, a cubic structure at room temperature. However, halide perovskites in the cubic phase have been shown to have significant local octahedral tilts, resembling lower temperature structures [4, 8, 9]. For this reason, we have used the polymorphous model of the cubic structure to study the STE. Nevertheless, it is useful to test if the low-temperature tetragonal structure leads to similar properties of the STE, as it displays similar local tilts as the dynamical cubic structure. Therefore, we performed additional TD-PBE0(28%) calculations on a tetragonal supercell. The test has been done using only the Γ point. The comparison between the transitions achieved in the polymorphous and tetragonal supercells is given in Figure 9.

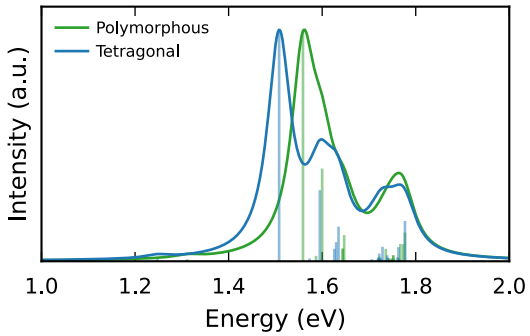

Figure 9: Transitions related to the STE in the polymorphous and tetragonal cells. The broadened spectra were generated by convolution with Lorentzians with a width of 0.03 eV. Calculations were performed considering the Γ point only.

7 STE emission in PBE0(28%) vs. DDH

We test the effect of the choice of the hybrid functional on the transitions related to the STE. In Figure 10 we compare the results achieved with the TD-PBE0(28%) and TD-DDH methods. Using TD-PBE0(28%), the transitions are found at energies lower by about 0.14 eV than in TD-DDH, consistent with the differences in the absorption spectra in the pristine material found within these two methods.

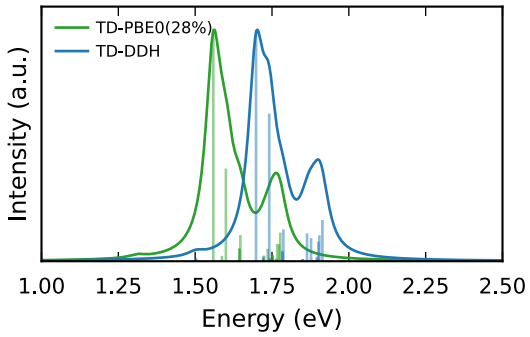

Figure 10: Transitions related to the STE calculated within the TD-PBE0(28%) and TD-DDH methods The broadened spectra were generated by convolution with Lorentzians with a width of 0.03 eV. Calculations were performed considering the Γ point only.

References

[1] Georg Kresse and Jürgen Hafner. Ab initio molecular dynamics for liquid metals. *Phys. Rev. B*, 47(1):558, 1993.

[2] Georg Kresse and Jürgen Furthmüller. Efficient iterative schemes for ab initio total-energy calculations using a plane-wave basis set. *Phys. Rev. B*, 54(16):11169, 1996.

[3] Haowei Peng, Zeng-Hui Yang, John P Perdew, and Jianwei Sun. Versatile van der Waals density functional based on a meta-generalized gradient approximation. *Phys. Rev. X*, 6(4):041005, 2016.

[4] Julia Wiktor, Erik Fransson, Dominik Kubicki, and Paul Erhart. Quantifying dynamic tilting in halide perovskites: Chemical trends and local correlations. *Chem. Mater.*, 35(17):6737–6744, 2023.

[5] Haiyuan Wang, Runhai Ouyang, Wei Chen, and Alfredo Pasquarello. High-quality data enabling universality of band gap descriptor and discovery of photovoltaic perovskites. *J. Am. Chem. Soc.*, 2024.

[6] Raisa-Ioana Biega, Marina R Filip, Linn Leppert, and Jeffrey B Neaton. Chemically localized resonant excitons in silver–pnictogen halide double perovskites. *J. Phys. Chem. Lett.*, 12(8):2057–2063, 2021.

[7] Maurizia Palummo, Eduardo Berrios, Daniele Varsano, and Giacomo Giorgi. Optical properties of lead-free double perovskites by ab initio excited-state methods. *ACS Energy Lett.*, 5(2):457–463, 2020.

[8] Julia Wiktor, Ursula Rothlisberger, and Alfredo Pasquarello. Predictive determination of band gaps of inorganic halide perovskites. *J. Phys. Chem. Lett.*, 8(22):5507–5512, 2017.

[9] Xin-Gang Zhao, Gustavo M Dalpian, Zhi Wang, and Alex Zunger. Polymorphous nature of cubic halide perovskites. *Phys. Rev. B*, 101(15):155137, 2020.